Mon. Not. R. Astron. Soc. **325,** L1–L5 (2001)

Magnetorotational instability in a rotating liquid metal annulus

Hantao Ji,[1]★ Jeremy Goodman[2] and Akira Kageyama[1,3]
[1]*Princeton Plasma Physics Laboratory, Princeton, NJ 08543, USA*
[2]*Princeton University Observatory, Princeton, NJ 08544, USA*
[3]*National Institute for Fusion Science, Toki, Gifu 509-5292, Japan*

Accepted 2001 May 10. Received 2001 May 8; in original form 2001 March 22

ABSTRACT

Although the magnetorotational instability (MRI) has been widely accepted as a powerful accretion mechanism in magnetized accretion discs, it has not been realized in the laboratory. The possibility of studying MRI in a rotating liquid metal annulus (Couette flow) is explored by local and global stability analysis. Stability diagrams are drawn in dimensionless parameters, and also in terms of the angular velocities at the inner and outer cylinders. It is shown that MRI can be triggered in a moderately rapidly rotating table-top apparatus, using easy-to-handle metals such as gallium. Practical issues of this proposed experiment are discussed.

Key words: accretion, accretion discs – instabilities – magnetic fields – MHD – planetary systems: protoplanetary discs – Galaxy: disc.

1 INTRODUCTION

Astrophysical magnetic fields have long been recognized to be important but difficult to understand. A prominent example concerns accretion discs (Shakura & Sunyaev 1973; Lynden-Bell & Pringle 1974), where orbiting plasmas gradually accrete on to a central mass. Three types of central object occur: protostars (stars in formation), collapsed stars in binary systems (white dwarfs, neutron stars and black holes), and supermassive black holes in active galactic nuclei (quasars etc.). In addition to the accretion process, jets and other spectacular phenomena may be magnetically driven by the disc (e.g. Meier, Koide & Uchida 2001). Understanding the dynamics and dissipation mechanisms in accretion discs holds an important key to understanding many active astronomical systems as a whole.

The accretion rates cannot be due to ordinary molecular or plasma viscosity because of the extraordinarily high Reynolds numbers involved. Theorists have often appealed to hydrodynamic turbulence (Pringle 1981), but recent numerical simulations indicate that non-magnetic discs are stabilized by their positive angular momentum gradient (Balbus, Hawley & Stone 1996; Cabot 1996; Hawley, Balbus & Winters 1999); in effect, Rayleigh's stability criterion appears to suppress local non-axisymmetric as well as axisymmetric disturbances (Rayleigh 1916). Linear axisymmetric instability of a *magnetized* but Rayleigh-stable fluid, the magnetorotational instability (MRI), was discovered decades ago (Velikhov 1959; Chandrasekhar 1960) but did not come to the attention of the astrophysical community until recently rediscovered (Balbus & Hawley 1991a), despite general recognition that magnetic effects might somehow be important (Shakura & Sunyaev 1973). Since then, many analytic and numerical studies of the MRI have been performed under increasingly complex and realistic assumptions, including such effects as finite resistivity, global boundary conditions, and nonlinearity in two and three dimensions (Balbus & Hawley 1991b; Curry, Pudritz & Sutherland 1994; Blaes & Balbus 1994; Brandenburg et al. 1995; Matsumoto & Tajima 1995; Hawley, Gammie & Balbus 1996; Stone et al. 1996; Gammie 1996; Jin 1996; Sano & Miyama 1999; Fleming, Stone & Hawley 2000; Hawley 2000).

Despite its popularity and importance, however, the MRI has never been realized in the laboratory or demonstrated observationally. Laboratory plasma experiments are primarily magnetically driven, and the observed flows, often induced as secondary effects of other instabilities, are small compared with the Alfvén speed. On the other hand, the existing body of experimental work on magnetized Couette flow using liquid metals (Donnelly & Ozima 1960, 1962; Donnelly & Caldwell 1964; Brahme 1970) has focused on magnetic stabilization of the Rayleigh instability, as first analysed by Chandrasekhar (1961). In this Letter, we explore the feasibility of a Couette flow experiment dedicated to MRI.

2 LOCAL STABILITY ANALYSIS

Couette flow involves a liquid confined between rotating coaxial cylinders (Couette 1890). Let their radii be $r_1 < r_2$, and their angular velocities Ω_1, Ω_2. In steady state, the radial angular momentum flux, $h \times 2\pi r \times \rho\nu \times r^2(-\partial\Omega/\partial r)$, is constant with radius, where h is the depth of the liquid, ρ is its density, and ν is its kinematic viscosity. If $\partial h/\partial r = 0$, then the angular velocity of the

★E-mail: hji@pppl.gov

liquid satisfies $r^3\partial\Omega/\partial r =$ constant, so that

$$\Omega(r) = a + \frac{b}{r^2}, \tag{1}$$

where $a = (\Omega_2 r_2^2 - \Omega_1 r_1^2)/(r_2^2 - r_1^2)$ and $b = r_1^2 r_2^2(\Omega_1 - \Omega_2)/(r_2^2 - r_1^2)$. The Rayleigh stability criterion is $a\Omega > 0$.

The dynamics of liquid metals is well described by the incompressible and dissipative magnetohydrodynamic (MHD) equations,

$$0 = \nabla \cdot \boldsymbol{V},$$

$$0 = \nabla \cdot \boldsymbol{B},$$

$$\frac{\partial \boldsymbol{B}}{\partial t} = \nabla \times (\boldsymbol{V} \times \boldsymbol{B}) + \eta \nabla^2 \boldsymbol{B},$$

$$\frac{\partial \boldsymbol{V}}{\partial t} + (\boldsymbol{V} \cdot \nabla)\boldsymbol{V} = \frac{(\boldsymbol{B} \cdot \nabla)\boldsymbol{B}}{\mu_0 \rho} - \frac{1}{\rho}\nabla\left(p + \frac{B^2}{2\mu_0}\right) + \nu \nabla^2 \boldsymbol{V},$$

where $\boldsymbol{V}$ is velocity, $\boldsymbol{B}$ is magnetic field, η is magnetic diffusivity, and p is a scalar potential incorporating both pressure and gravity. In cylindrical coordinates, the equilibrium quantities are $\boldsymbol{B}_0 = (0, 0, B)$ and $\boldsymbol{V}_0 = (0, r\Omega, 0)$, and the balance of forces is $\partial p_0/\partial z = 0$ and $\partial p_0/\partial r = \rho r \Omega^2$.

WKB methods describe the stability of this system very well even on the largest scales. Using cylindrical coordinates, the perturbations are $\boldsymbol{B}_1 = (B_r, B_\theta, B_z)$ and $\boldsymbol{V}_1 = (V_r, V_\theta, V_z)$, all proportional to $\exp(\gamma t - \mathrm{i}k_z z - \mathrm{i}k_r r)$, so that γ is the growth rate and the perturbations are axisymmetric. The minimum k_z and k_r are assumed to be π/h and $\pi/(r_2 - r_1)$, respectively, so that the total wavenumber $k = \sqrt{k_z^2 + k_r^2} = k_z\sqrt{1 + \epsilon^2}$, where $\epsilon \equiv h/(r_2 - r_1)$ is the elongation of a toroidal cross-section of the liquid metal annulus. The linearized equations of motion are

$$0 = k_r V_r + k_z V_z,$$

$$0 = k_r B_r + k_z B_z,$$

$$\gamma B_r = -\mathrm{i}k_z B V_r - \eta k^2 B_r,$$

$$\gamma B_\theta = -\mathrm{i}k_z B V_\theta + \frac{\partial \Omega}{\partial \ln r} B_r - \eta k^2 B_\theta,$$

$$\gamma V_r - 2\Omega V_\theta = -\mathrm{i}\frac{k_z B}{\mu_0 \rho} B_r + \mathrm{i}\frac{k_r}{\rho} p_1 + \mathrm{i}\frac{k_r B}{\mu_0 \rho} B_z - \nu k^2 V_r,$$

$$\gamma V_\theta + \frac{\kappa^2}{2\Omega} V_r = -\mathrm{i}\frac{k_z B}{\mu_0 \rho} B_\theta - \nu k^2 V_\theta,$$

$$\gamma V_z = \mathrm{i}\frac{k_z}{\rho} p_1 - \nu k^2 V_z,$$

where the epicyclic frequency is defined by $\kappa^2 \equiv (1/r^3)\partial(r^4\Omega^2)/\partial r = 4\Omega^2 + \partial\Omega^2/\partial \ln r$ and p_1 is the perturbed pressure. The vertical induction equation is not needed since B_z can be deduced from $\nabla \cdot \boldsymbol{B} = 0$. These equations lead to the following dispersion relation:

$$[(\gamma + \nu k^2)(\gamma + \eta k^2) + (k_z V_\mathrm{A})^2]^2 \frac{k^2}{k_z^2} + \kappa^2(\gamma + \eta k^2)^2 + \frac{\partial \Omega^2}{\partial \ln r}(k_z V_\mathrm{A})^2 = 0.$$

The Alfvén speed is $V_\mathrm{A} \equiv B/\sqrt{\mu_0 \rho}$. This dispersion relation is identical to the one derived for accretion discs in the incompressible limit (Sano & Miyama 1999).

Introducing a dimensionless vorticity parameter, $\zeta \equiv (1/r\Omega)\partial(r^2\Omega)/\partial r = 2 + \partial \ln \Omega/\partial \ln r$, we have $\kappa^2 = 2\Omega^2\zeta$ so that the Rayleigh stability criterion becomes $\zeta \geq 0$. Similarly, $\partial\Omega^2/\partial \ln r = 2\Omega^2(\zeta - 2)$. There are three other relevant frequencies: resistive, $\omega_\eta \equiv \eta k^2$; viscous, $\omega_\nu \equiv \nu k^2$; and Alfvénic, $\omega_\mathrm{A} \equiv |k_z V_\mathrm{A}|$. Because liquid metals are far more resistive than viscous, ω_η serves as a base frequency in the following three dimensionless parameters: magnetic Prandtl number, $P_\mathrm{m} \equiv \omega_\nu/\omega_\eta$; Lundquist number, $S \equiv \omega_\mathrm{A}/\omega_\eta$; and magnetic Reynolds number, $R_\mathrm{m} \equiv \Omega/\omega_\eta$. The astrophysical literature gives several inequivalent definitions of 'magnetic Reynolds number', some corresponding to our S. Some involve the sound speed, c_s, for, although MRI is essentially non-compressive, vertical force balance in an astrophysical disc relates c_s to the half-thickness: $c_\mathrm{s} \approx h\Omega$. The free energy for MRI derives from differential rotation, represented in our dimensionless system by a combination of ζ and R_m; however, magnetic field, represented by S, is required to liberate this energy from hydrodynamic constraints.

Using the normalized growth rate, $\gamma/\omega_\eta \to \gamma$, the dispersion relation can be rewritten as

$$[(\gamma + P_\mathrm{m})(\gamma + 1) + S^2]^2(1 + \epsilon^2) + 2\zeta R_\mathrm{m}^2(\gamma + 1)^2 - 2(2 - \zeta)R_\mathrm{m}^2 S^2 = 0.$$

It can be shown that there are no purely imaginary roots for γ, as follows. Suppose that $\gamma = \mathrm{i}\omega$ for real and non-zero ω. From the imaginary part of the equation above, one finds

$$\omega^2 = S^2 + P_\mathrm{m} + (1 + P_\mathrm{m})\zeta\sigma^2, \qquad \sigma \equiv \frac{R_\mathrm{m}}{1 + P_\mathrm{m}}\sqrt{\frac{2}{1 + \epsilon^2}}.$$

Substituting this into the real part yields

$$\sigma^4\zeta^2 + 2\sigma^2\zeta + 1 + \frac{S^2}{P_\mathrm{m}} + 2\frac{S\sigma^2}{P_\mathrm{m}} = 0.$$

This is a quadratic equation in ζ which must be real. However, the discriminant

$$-\sigma^4\left(\frac{S^2}{P_\mathrm{m}} + 2\frac{S\sigma^2}{P_\mathrm{m}}\right)$$

is negative unless $S = 0$ or $R_\mathrm{m} = 0$. Hence there are no purely oscillatory modes. On the other hand, all roots of the dispersion relation for γ have negative real parts as $R_\mathrm{m} \to 0$ (non-rotating flow). Hence the transition to instability occurs through $\gamma = 0$, and the necessary and sufficient condition for stability is that the value of the dispersion relation at $\gamma = 0$ remain positive as R_m increases:

$$(P_\mathrm{m} + S^2)^2(1 + \epsilon^2) + 2\zeta R_\mathrm{m}^2 - 2(2 - \zeta)R_\mathrm{m}^2 S^2 \geq 0, \tag{2}$$

which can be taken into various limits.

(i) Non-magnetic limit. As $\eta \to \infty$, the three terms S^4, $R_\mathrm{m}S^2$ and $R_\mathrm{m}^2 S^2$ approach zero faster than the others, leading to the stability condition $P_\mathrm{m}^2(1 + \epsilon^2) + 2\zeta R_\mathrm{m}^2 \geq 0$. Stability occurs when $\zeta \geq 0$, and also when $\zeta < 0$ if the Taylor number-like expression $-2\zeta\Omega^2/\nu^2 k^4 \leq 1 + \epsilon^2$ (Taylor 1923).

(ii) Ideal MHD limit. As $\eta \to 0$, the other two terms dominate, with stability for $S^2(1 + \epsilon^2) \geq 2(2 - \zeta)R_\mathrm{m}^2$. Instability occurs at sufficiently weak fields (small S) unless $\zeta \geq 2$, i.e. $\partial \ln \Omega/\partial \ln r \geq 0$ (Balbus & Hawley 1991a).

(iii) Small-P_m limit. In liquid metals, usually viscosity is much smaller than resistivity, $P_\mathrm{m} \sim 10^{-6}$. As $P_\mathrm{m} \to 0$, equation (2)

reduces to

$$\zeta \geq \frac{2S^2}{S^2+1} - \frac{S^4(1+\epsilon^2)}{2R_{\rm m}^2(S^2+1).} \tag{3}$$

3 STABILITY DIAGRAMS AND GROWTH RATES

The stability condition (3) defines a two-dimensional surface in the parameter space (S, ζ, $R_{\rm m}$) at fixed ϵ. To illustrate the dependence on these parameters, we vary only two of them at a time. Stability boundaries in the (ζ, S) plane are shown in Fig. 1 for the case of $\epsilon = 1$. When $\zeta < 0$, the annulus is unstable hydrodynamically to the Rayleigh mode at $S = 0$ but can be stabilized (Chandrasekhar 1961) by a large magnetic field (large S). When $\zeta > 0$, the annulus is stable at zero field but unstable at some $S > 0$ if $R_{\rm m}$ is large enough. Stability returns at even larger S. The unstable region extends to larger S and ζ at larger $R_{\rm m}$. Stability at $S = 0$ and stability as $S \rightarrow \infty$ are hallmarks of MRI (Balbus & Hawley 1991a, 1998). (In ideal MHD, instability extends formally to $S = 0^+$.) It can be seen that there is a maximum ζ above which MRI is absent for a given $R_{\rm m}$. From equation (3),

$$\zeta_{\rm max} = 2 - \frac{1+\epsilon^2}{R_{\rm m}^2}\left(\sqrt{1+\frac{4R_{\rm m}^2}{1+\epsilon^2}} - 1\right) \tag{4}$$

at the S-value given by $S^2 = \sqrt{1 + 4R_{\rm m}^2/(1+\epsilon^2)} - 1$.

Fig. 2 shows stability in the $(\zeta, R_{\rm m})$ plane. Region (I) is hydrodynamically unstable but can be stabilized by a finite magnetic field. This region has been extensively studied both theoretically and experimentally (Chandrasekhar 1961), and is exemplified by point B. Region (II) is hydrodynamically stable but

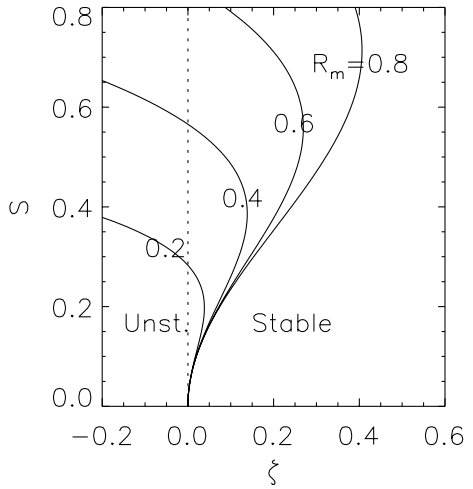

Figure 1. Stability of a rotating liquid metal annulus in dimensionless parameter space of (ζ, S) at a few values of $R_{\rm m}$ for the case of $\epsilon = 1$. Areas to the right of the curves indicate stability.

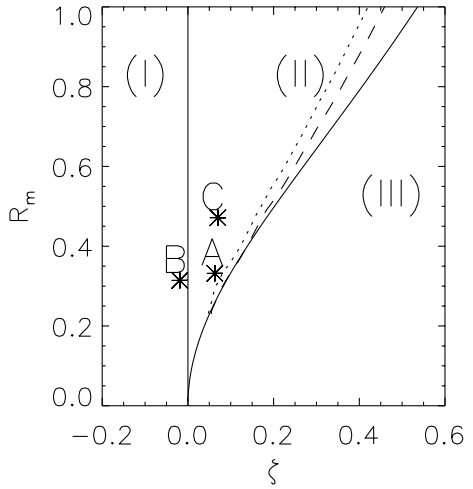

Figure 2. Stability of a rotating liquid metal annulus in (ζ, R) space. Here the stability can be divided into three regions: region (I) is hydrodynamically unstable but can be stabilized by a finite magnetic field, as exemplified by point B. Region (II) is hydrodynamically stable but can be destabilized by the presence of a magnetic field (MRI), as exemplified by points A and C. Region (III) is always stable. Results from global eigenmode analysis are also shown: a dotted line for conducting boundary conditions and a dashed line for insulating boundary conditions.

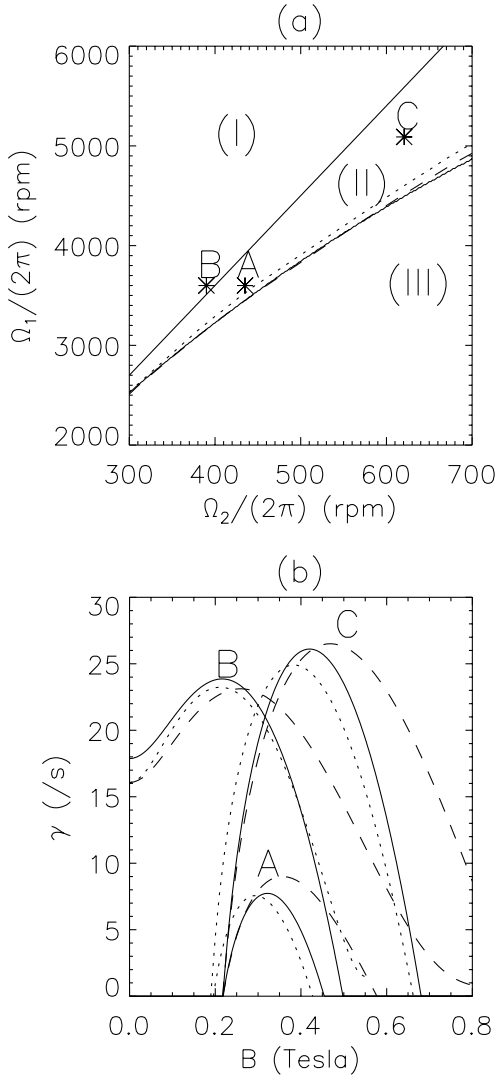

Figure 3. Stability diagram of a rotating gallium annulus in (Ω_2, Ω_1) space with dimensions $r_1 = 0.05$ m, $r_2 = 0.15$ m and $h = 0.1$ m. The growth rates of points A, B and C, corresponding to those in Fig. 2, are also shown as functions of magnetic field in (b). Results from global eigenmode analysis are also shown: dotted lines for conducting boundary conditions and dashed lines for insulating boundary conditions.

destabilized by a magnetic field. This is the MRI region, and has never been studied experimentally. Growth rates at points A and C are given below. Region (III) is always stable. The boundary between regions (II) and (III) is given by equation (4).

It is useful to project the stability diagram on to experimentally controllable parameters. To apply the local dispersion relation, we take $\zeta = 2a/\bar{\Omega}$ (from equation 1) and $R_{\rm m} \equiv \bar{\Omega}/\omega_\eta$, with $\bar{\Omega} \equiv \sqrt{\Omega_1 \Omega_2}$. Fig. 3(a) shows stability in the (Ω_2, Ω_1) plane for an annulus of dimensions $r_1 = 0.05\,{\rm m}$, $r_2 = 0.15\,{\rm m}$ and $h = 0.1\,{\rm m}$ (hence $\epsilon = 1$) filled with gallium ($\rho \simeq 6 \times 10^3\,{\rm kg\,m^{-3}}$, $\eta \simeq 0.2\,{\rm m^2\,s^{-1}}$, $\nu \simeq 3 \times 10^{-7}\,{\rm m^2\,s^{-1}}$). Table 1 lists the physical parameters at points A, B and C. The corresponding growth rates are shown as functions of magnetic field in Fig. 3(b).

The applicability of WKB is subject to doubt, since the most unstable wavelengths are larger than the gap width and cylinder height. In fact, global analysis shows that the eigenfunctions are non-sinusoidal and sensitive to the boundary conditions. Yet the growth rates are remarkably robust. A linearized, finite-difference, initial-value code was written to detect the fastest growing mode. Periodic boundary conditions were used in z. Radial boundaries were impenetrable and no-slip ($\delta V_1 = 0$), and electrically either perfectly insulating or perfectly conducting. The results are compared with the WKB analysis in Figs 2 and 3. Fig. 4 shows eigenmodes for the parameters of point C with $B = 0.3$ tesla. Differences between the conducting and insulating cases can be seen near the inner boundaries. A Hartmann layer (Hartmann 1937), consisting of large toroidal and axial velocities within a radial thickness of $\sim\sqrt{\nu\eta}/V_{\rm A} < 1\,{\rm mm}$ (not visible in Fig. 4), forms at the inner conducting boundary as the Lorentz force, $\delta j_r \times B_z$, balances with the viscous force. Nevertheless, the growth rates are remarkably similar to those of the local analysis, which therefore should suffice for preliminary experimental design. [Details of the global analysis will be reported elsewhere (Goodman & Ji 2001).]

Table 1. Parameters for a gallium annulus with $r_1 = 0.05\,{\rm m}$, $r_2 = 0.15\,{\rm m}$ and $h = 0.1\,{\rm m}$.

Point	Ω_1(rpm)	Ω_2(rpm)	$R_{\rm m}$	ζ
A	3600.00	435.00	0.3319	0.062 93
B	3600.00	390.00	0.3143	−0.018 99
C	5089.77	620.70	0.4715	0.069 84

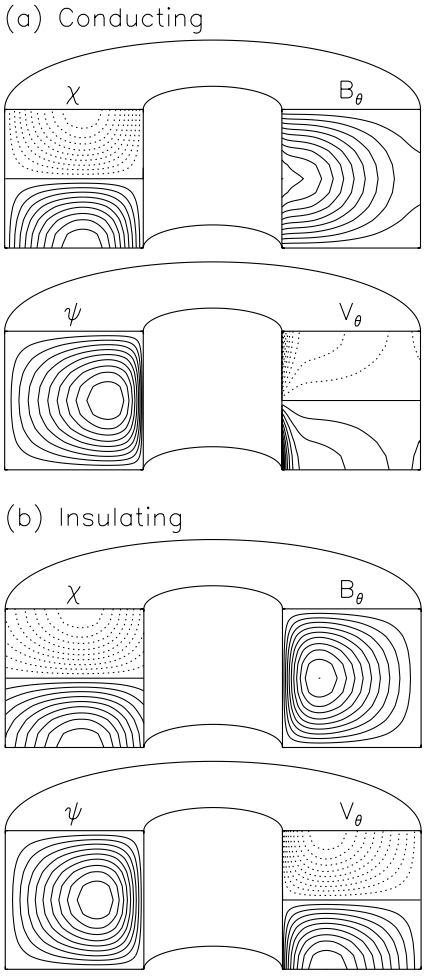

Figure 4. Eigenmodes for conditions given by point C in Fig. 3 at $B = 0.3$ tesla with conducting (a) and insulating (b) radial boundaries. Here, solid (dotted) lines represent positive (negative) values; χ and ψ are poloidal flux and stream functions, respectively.

A fully non-linear incompressible MHD code has been developed to study the problem in three dimensions (Kageyama, Ji & Goodman, in preparation). Initial results from linear and two-dimensional runs of this code with conducting, freely-slipping boundary conditions agree with the local and global analyses. For example, for the conditions given by point C in Figs 2 and 3 at $B = 0.3$ tesla, the growth rate is $21.67\,{\rm s^{-1}}$ from simulations, $21.90\,{\rm s^{-1}}$ from global analysis, and $19.10\,{\rm s^{-1}}$ from local analysis.

4 DISCUSSION AND CONCLUSIONS

Several issues must be explored before committing to an experimental design. The first is geometric optimization with regard to aspect ratio [$A \equiv (r_2 + r_1)/(r_2 - r_1)$] and elongation [$\epsilon \equiv h/(r_2 - r_1)$]. Obviously, $\epsilon \sim 1$ is desirable to minimize volume, and therefore expense, at a given growth rate. Less obviously, aspect ratios close to unity cause the eigenmodes and growth rates to be dominated by the inner cylinder, which is undesirable if the aim is to imitate relatively uniform local conditions within an astrophysical disc. Therefore moderate values of $A(\sim 2)$ and $\epsilon(\sim 1)$ are preferred.

The periodic vertical boundary conditions used in all of our analyses take no account of viscous layers at the top and bottom of the flow. (The top will have to be capped because of large radial pressure gradients.) The main effect of these viscous boundary layers is to drive Ekman circulation, which flows more rapidly against a weak angular momentum gradient than against uniform rotation. The thickness of the Ekman layer $\delta_{\rm E} \approx \zeta^{-1/4}\sqrt{\nu/\bar{\Omega}}$ is small ($\sim 10^{-3}\,h$ at point C), and the Ekman circulation time $\zeta^{3/4} h/\sqrt{\nu\bar{\Omega}} \sim 2\,{\rm s}$ is much longer than a typical MRI growth time, so we do not expect these layers to be important for stability. To minimize their effect further, if necessary, one could increase ϵ, use differentially rotating rings at the vertical boundaries, or modify the boundary layer by localized Lorentz forces (Brahme 1970).

A third issue is finite-amplitude or non-linear hydrodynamical instability in Rayleigh-stable regimes. Few theoretical studies on this subject exist (Serrin 1959; Joseph & Munson 1970). It has been argued from experiments that a rapid Couette flow can be non-linearly unstable (Richard & Zahn 1999). However, there are indications that such instabilities are caused by wall surface defects (Schultz-Grunow 1959), which can be minimized. In fact, it has been shown numerically that a positive angular momentum gradient strongly resists non-linear instability (Balbus et al. 1996;

Hawley et al. 1999). The outcome depends, however, on the amplitude of the initial perturbation and the strength of the angular momentum gradient. These questions could be addressed empirically and relatively inexpensively in prototype experiments using water.

One would like to predict the non-linear phases of MRI in the laboratory system. Ultimately, non-linear MRI is closely related to other important physics of accretion discs involving magnetic field, i.e. dynamo processes and jet formation. Ongoing three-dimensional MHD simulations (Kageyama, Ji & Goodman, in preparation) will provide useful insights here. Indeed, an important purpose of the experiment is to be a testbed for MHD codes since, lacking detailed observational constraints, theorists depend upon computer simulations to understand MRI-driven turbulence.

The experiment will be far more resistive than most accretion discs, although perhaps not all (Gammie 1996; Gammie & Menou 1998). Simulations indicate that when the field is generated by the disc itself (magnetic dynamo), then the large-scale field is nearly toroidal, the important instabilities are non-axisymmetric, and the turbulence sustains itself only if S and $R_{\rm m}$ are much larger than the experiment proposed here will achieve (Balbus & Hawley 1991b; Brandenburg et al. 1995; Hawley et al. 1996; Sano, Inutsuku & Miyama 1998; Fleming et al. 2000). On the other hand, the innermost (and therefore most energetic) parts of accretion discs often encounter a vertical field as a result of the central compact object. The works cited above find that, in the presence of an imposed vertical field, turbulence is driven by axisymmetric modes and persists to higher resistivity, probably into the experimentally accessible regime.

In summary, we have used linear stability analyses to explore the prospects for magnetorotational instability in a magnetized Couette flow. We find that MRI can be achieved in a moderately rapidly rotating table-top apparatus using an easy-to-handle liquid metal such as gallium. Auxiliary experiments with an inexpensive non-magnetic fluid, such as water, will be valuable both as prototypes and as controls to distinguish MRI from non-linear hydrodynamic instabilities. The onset and dynamics of MRI can be detected by torque measurements of cylinders and magnetic sensors placed around the annulus. Ultrasonic imaging may also be possible. If successful, this will be a rare example of a MHD astrophysical process that can be studied in the laboratory.

ACKNOWLEDGMENTS

The authors are grateful to Drs. P. Diamond, R. Goldston, S. Hsu, R. Kulsrud, W. Tang and M. Yamada for fruitful discussions. We thank our anonymous referee for valuable comments, especially on the oscillatory modes. This work is supported by the US Department of Energy and by NASA grant NAG5-8385 (to JG).

REFERENCES

Balbus S. A., Hawley J. F., 1991a, ApJ, 376, 214
Balbus S. A., Hawley J. F., 1991b, ApJ, 376, 223
Balbus S. A., Hawley J. F., 1998, Rev. Mod. Phys., 70, 1
Balbus S. A., Hawley J. F., Stone J. M., 1996, ApJ, 467, 76
Blaes O. M., Balbus S. A., 1994, ApJ, 421, 163
Brahme A., 1970, Phys. Scr., 2, 108
Brandenburg A., Nordlund Å., Stein R. F., Torkelsson U., 1995, ApJ, 446, 741
Cabot W., 1996, ApJ, 465, 874
Chandrasekhar S., 1960, Proc. Natl. Acad. Sci., 46, 253
Chandrasekhar S., 1961, Hydrodynamic and Hydromagnetic Stability. Oxford Univ. Press, London
Couette T., 1890, Ann. Chim. Phys., 21, 433
Curry C., Pudritz R. E., Sutherland P. G., 1994, ApJ, 434, 206
Donnelly R. J., Caldwell D. R., 1964, J. Fluid Mech., 19, 257
Donnelly R. J., Ozima M., 1960, Phys. Rev. Lett., 4, 497
Donnelly R. J., Ozima M., 1962, Proc. Soc. Lond. A, 266, 272
Fleming T. P., Stone J. M., Hawley J. F., 2000, ApJ, 530, 464
Gammie C. F., 1996, ApJ, 457, 355
Gammie C. F., Menou K., 1998, ApJ, 492, L75
Goodman J., Ji H., 2001, J. Fluid Mech., submitted
Hartmann J., 1937, Mat-Fys. Medd., 15, 6
Hawley J. F., 2000, ApJ, 528, 462
Hawley J. F., Gammie C. F., Balbus S. A., 1996, ApJ, 464, 690
Hawley J. F., Balbus S. A., Winters W. F., 1999, ApJ, 518, 394
Jin L., 1996, ApJ, 457, 798
Joseph D. D., Munson B. R., 1970, J. Fluid Mech., 43, 545
Lynden-Bell D., Pringle J. E., 1974, MNRAS, 168, 603
Matsumoto R., Tajima T., 1995, ApJ, 445, 767
Meier D. L., Koide S., Uchida Y., 2001, Sci, 291, 84
Pringle J. E., 1981, ARA&A, 19, 137
Rayleigh L., 1916, Proc. Soc. Lond. A, 93, 148
Richard S., Zahn J. P., 1999, A&A, 347, 734
Sano T., Miyama S., 1999, ApJ, 515, 776
Sano T., Inutsuku S., Miyama S., 1998, ApJ, 506, L57
Schultz-Grunow F., 1959, Z. Angew. Math. Mech., 39, 101
Serrin J., 1959, Arch. Ration. Mech. Anal., 3, 1
Shakura N. I., Sunyaev R. A., 1973, A&A, 24, 337
Stone J. M., Hawley J. F., Gammie C. F., Balbus S. A., 1996, ApJ, 463, 656
Taylor G. I., 1923, Phil. Trans. R. Soc. Lond. A, 223, 289
Velikhov E. P., 1959, Sov. Phys. JETP, 36, 995

This paper has been typeset from a TEX/LATEX file prepared by the author.